

Some simulation of the Daya Bay calibration system

J. Liu, C. J. Jillings, R. D. McKeown
California Institute of Technology

October 8, 2006

Contents

1	How to calibrate various detector parameters with radioactive sources	1
1.1	Change of attenuation length	2
1.2	Change of scintillation yield	2
1.3	Steel Tank Surface Reflectivity	3
1.4	Acrylic Vessel Attenuation	3
2	Effects of various optical parameters to the n capture spectrum	5
3	Effect of various optical parameters to the positron spectrum	6
3.1	point-point to uniform photon yield	7
3.2	Positron Efficiency	9
3.3	Positron Spectrum Distortion	9
4	Conclusion	10

Abstract

In this note, we present some simulation studies of the sensitivity of the 20 ton, 3-zone Daya Bay central detector module to various optical parameters of the detector, and propose to use different radioactive sources to calibrate these parameters. A quantitative study is then made on how well one could calibrate (relatively) the neutron and positron spectra among various detectors.

1 How to calibrate various detector parameters with radioactive sources

Three sources have been chosen in this study: ^{68}Ge , ^{60}Co , and Americium-Beryllium (AmBe). The ^{68}Ge and ^{60}Co produce gamma rays. The AmBe source produces neutrons, which get captured by Gadolinium or protons in the liquid scintillator, and subsequently produce delayed ($\sim 20 \mu\text{s}$) gamma rays*. The photon energies of the three sources are summarized in Table 1. Due to their fixed photon energy, these sources are ideal to calibrate detector energy response at the range we are interested in.

Source	Photon Energy (MeV)	Type
^{68}Ge	$0.511 \times 2 = 1.022$	prompt
^{60}Co	$1.173 + 1.333 = 2.506$	prompt
AmBe	8.023	2 to 3 γ s delayed

Table 1: *Gamma energy and characteristics of ^{68}Ge , ^{60}Co , and AmBe sources.*

In the rest of this section, we shall consider procedures to calibrate a few representative detector parameters. Each calibration measurement is designed with care, such that it is primarily sensitive to a certain parameter, although coupled effects from multiple parameters are inevitable.

*In the remainder of this note, we shall only consider the neutron (delayed) capture energy. A timing cut of $t > 1 \mu\text{s}$ is applied to the MC events to remove neutron's prompt energy loss through elastic scattering and thermalization.

1.1 Change of attenuation length

The change of light attenuation will change the signal uniformity throughout the detector. As an example, the n-Gd capture charge yield as a function of the vertex location are plotted as a 2D map in Fig. 1 for two detectors, with attenuation lengths 4.5 and 18 m, respectively. For simplicity, we have assumed the same attenuation length for the inner and outer detector volumes. As one would expect, the signal uniformity improves with increasing attenuation length.

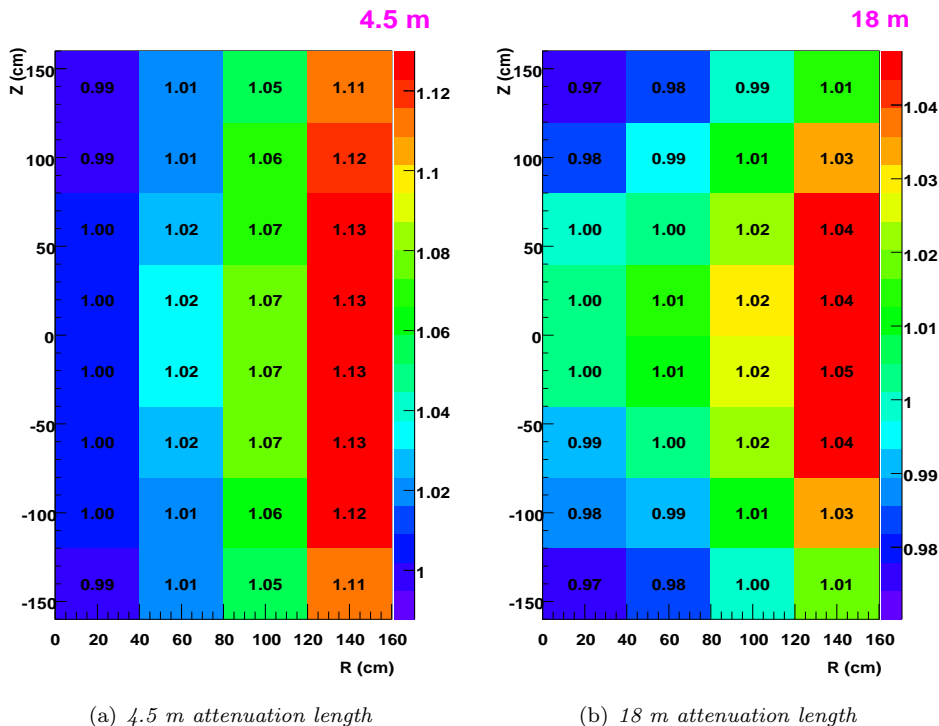


Figure 1: The n-Gd capture yield (normalized to the yield at detector) as a function of the neutron vertex (R, z).

Conversely, the n-Gd yield ratio between the “center” and “uniform” can be used as a measure of the scintillator attenuation length. In the real experiment, the “center” yield can be calibrated by putting an AmBe source at the center of the module, whereas the “uniform” yield is the average n-Gd capture signal from either the inverse beta or cosmogenic background[†]. In Fig. 2(a), this ratio from the simulation is plotted as a function of the attenuation length. If one takes 9 m as the nominal attenuation length, a 15% change around the nominal correspond to $\sim 0.5\%$ change in this ratio, which can be measured with 1000 “center” and “uniform” events. An alternative, and perhaps more sensitive approach, as suggested by the maps in Fig. 1, is to measure the “corner”/“center” yield ratio. In Fig. 2(b), this ratio for a ^{60}Co source[‡] is plotted against the attenuation length, where the “corner” corresponds to the source location of ($R = 140, z = 140$) cm. The same 15% change of the attenuation length from the nominal 9 m would result in a more than 1% change in this ratio, which again can be detected with 1000 “center” and “corner” ^{60}Co events.

1.2 Change of scintillation yield

Ignoring the small contribution from the Čerenkov photons, the total PE yield is directly proportional to the scintillation yield of the liquid scintillator. Therefore, a global change of the scintillation yield in the outer and inner detector volume can be trivially calibrated by, say, the total photon yield for a ^{60}Co source placed at the center of the detector. This is demonstrated in Fig. 3.

On the other hand, it is conceivable that the change of the scintillation yield happens, for example, only in the outer scintillator volume. To measure this change in the simulation, a ^{60}Co is placed at the inner edge of the outer liquid scintillator volume on the “equator”, and we choose to look at only the closest

[†]In this sense, the neutron “uniform” yield is self-calibrating

[‡]The ^{60}Co source is chosen, instead of an AmBe source, to have a better control over the true vertex position.

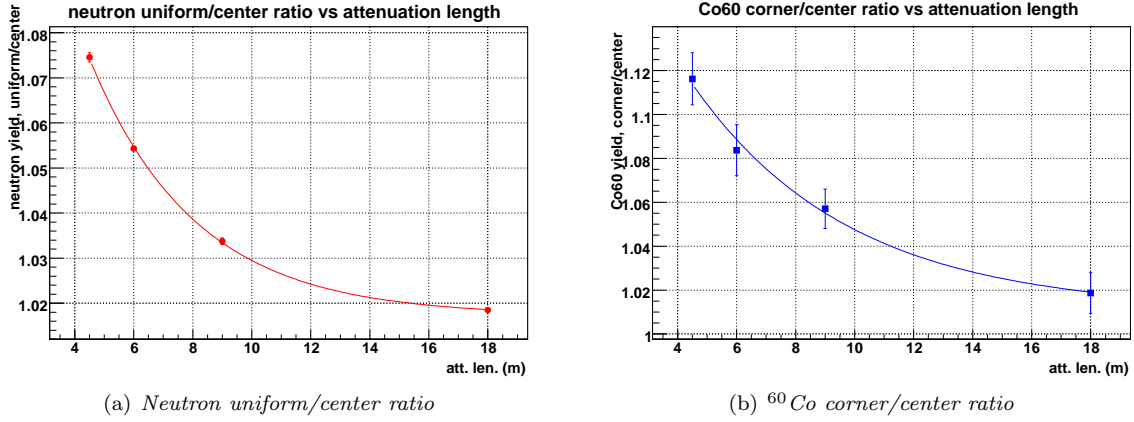


Figure 2: Two possible ways to measure the attenuation length: a) neutron uniform/center ratio, with error bars corresponding to 100,000 uniform and 10,000 center neutron events; b) ^{60}Co corner/center ratio, with 1000 corner and center events for each data point.

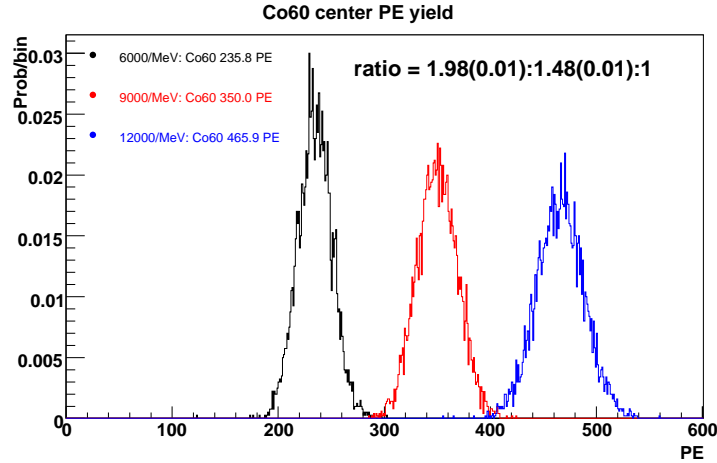


Figure 3: The ^{60}Co center spectra for various scintillation yield.

14 (“head-on”) phototubes to the source. This configuration is illustrated in Fig. 4. The reflected events are further eliminated by requiring the hit time less than 6.7 ns. The relatively short photon path lengths minimize the impact of light attenuation. Therefore, the summed direct PE yield from these head-on tubes is now primarily sensitive to the scintillation yield in the outer volume. The simulation is performed with three scintillation yield in the outer layer, with that of the inner layer is fixed, and the results are displayed in Fig. 5. Just to set the scale, a 10% change of the outer scintillation yield will lead to a 5% change of the head-on photon yield, which is measurable with 1000 ^{60}Co events.

1.3 Steel Tank Surface Reflectivity

In general, for a given source trigger, the photons reflected by the tank surface hits the PMTs later. Therefore, the ratio of the reflected to the direct hits should give a measure of the tank reflectivity. When the source is located at the center, the timing cut can be set approximately to 20 ns, corresponding to a direct path length of 3 m and an average index of fraction of 1.5. The ratios of the “reflected” and “direct” hits for three different refractivity, with a ^{60}Co source at the center, are plotted in Fig. 6. As one observes from the figure, if the reflectivity changes from 0.8 to 0.7, this ratio will decrease by 0.2, which is easily measurable with 1000 ^{60}Co events.

1.4 Acrylic Vessel Attenuation

Although in the baseline design, the thickness of the inner and outer acrylic vessels are both 1 cm, large variation of light attenuation can potentially affect the detector light yield. As an example, by changing

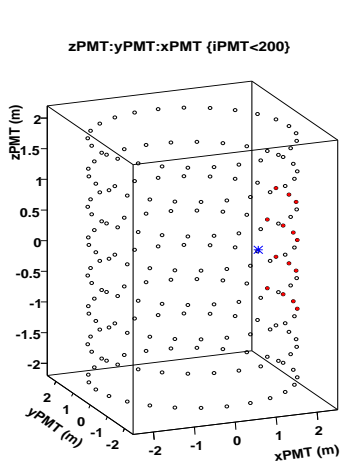


Figure 4: An illustration of source location on the closest 14 PMTs.

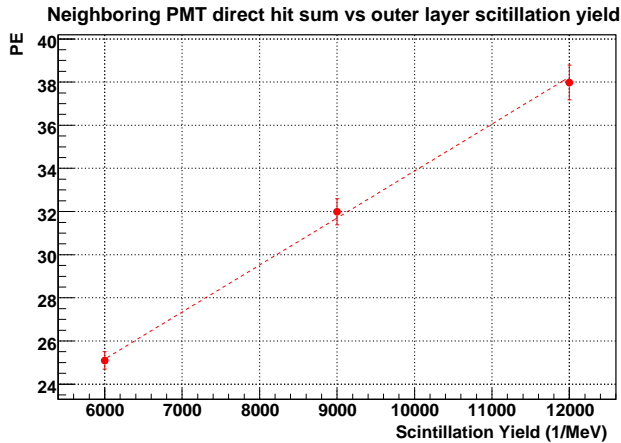


Figure 5: Sum of the direct hits from the 14 neighboring PMTs vs the scintillation yield of the outer scintillation layer.

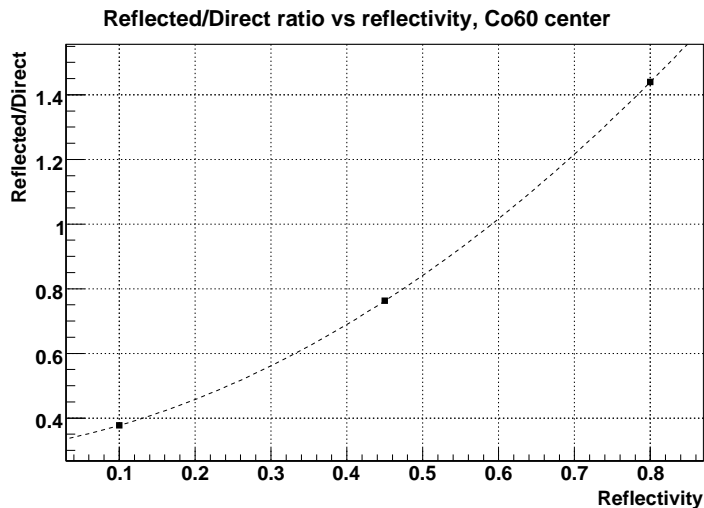


Figure 6: The average yield ratio for reflected and direct hits with a ^{60}Co source at the detector center.

the attenuation length for both the inner and outer acrylic from 5 to 0.2 m, the total light yield for a ^{60}Co source located at the edge of the inner detector decreases by 18% from 389.6 to 319.5 PEs, and the energy resolution degraded from 6.76% to 7.63%. However, only based on the total charge, it is very difficult to distinguish this effect from the change of other optical parameters.

Alternatively, we attempt a procedure very similar to that illustrated in Fig. 4. A ^{60}Co source is placed right inside or outside of the inner acrylic vessel. 10,000 MC events are generated for each in/out combination, and the in/out ratio of the summed yield for the 14 “head-on” PMTs are taken. Note that by taking the ratio, other optical properties are canceled. The ratio, corrected for the different solid angle for “in” and “out” locations, are tabulated in Table 2 for different inner acrylic attenuation lengths. The results is not conclusive.

In principle, if one puts the source right inside or outside of the outer acrylic vessel, examines the “head on” PMTs at the opposite side of the tank, and takes the out/in ratio instead, one gets a measure of the outer acrylic tank attenuation. This has not be studies quantitatively. In any case, due to the thin thickness, a reasonable variation of the acrylic attenuation, say 5 ± 1 m, will not produce significant systematic effect in the measured energy spectrum.

So far we have demonstrated that using a system with radioactive sources is capable to calibrate various

Inner acrylic attenuation length (m)	In/Out ratio (%)
5	99.9 (3.6)
2	99.9 (3.6)
1	95.7 (3.4)
0.5	1.01 (3.7)
0.2	97.9 (3.6)

Table 2: The “In/Out” ratio for various inner acrylic tank attenuation length.

optical properties of the detector. Ultimately, one would use these optical parameters to reconstruct reaction vertex and energy event by event, as well as tuning the MC to reproduce the data in real analysis. In the remainder of this note, however, we shall consider a very simple (vertex independent) energy reconstruction using the calibration data, and explore how well this works as a relative calibration for the neutron and positron spectra between two detectors.

2 Effects of various optical parameters to the n capture spectrum

The neutrons get captured by Gadolinium in the inner detector volume, and release two or more photons with a total “delayed” energy of ~ 8 MeV. In Fig. 8(a) below, some typical neutron delayed PE spectra for various attenuations are shown, where the low and high peaks correspond to the proton and Gadolinium captures, respectively. In the data analysis, one selects neutrons by placing a cut at 6 MeV, after converting the charge into visible energy. A consistent calibration scheme is needed to ensure an identical 6 MeV cut in different detectors, thereby an identical neutron detection efficiency.

To the first order, the location of the measured n-Gd peak give a consistent calibration of the energy scale among different detector. Assuming a linear energy response, determining the “6 MeV” is seemingly trivial. However, it is conceivable that the the non-linearity due to, for example, Birk’s quenching or Čerenkov, could be different for different detectors. Therefore, one should take the non-linearity into account to determine the 6 MeV. Furthermore, the dependence of light yield on the vertex location due to, for example, the light attenuation (Fig. 1), can lead to a relative difference in the spectrum shape among difference detectors. Therefore, simple peak fitting would lead to a biased energy scale, and one shall seek a more robust peak location determination.

To take the above two considerations into account, the following procedure is used to reconstruct the neutron energy spectrum:

- First, the energy non-linearity is calibrated by using ^{68}Ge , ^{60}Co and AmBe “center” data. The PE yield is fitted with a quadratic function: $NPE_{center} = a_0 + a_1E + a_2E^2$. The total charge per MeV for these three sources and the fit are shown in Fig. 7 for a typical detector.
- Second, the “center” calibration curve is scaled by some α_0 to roughly match the measured (“uniform”) n-Gd capture peak. This gives the new energy calibration relation: $NPE_{uniform} = \alpha_0(a_0 + a_1E + a_2E^2)$.
- Third, one tweaks the value of the scaling factor α_0 iteratively, until the mean of the “uniform” energy spectrum between [6,10] MeV is 8.0 MeV. This gives the final energy calibration relation: $NPE_{uniform} = \alpha(a_0 + a_1E + a_2E^2)$.
- Lastly, the 6 MeV cut is set according the energy calibration curve in the previous step.

Note that the third step is to define a consistent and model independent energy scale. For demonstration purpose, the raw PE and the reconstructed energy spectra for four different attenuation lengths (4.5, 6, 9, and 18 m) are shown in Fig. 8.

To evaluate this procedure quantitatively, three optical parameters are varied: the scintillation yield (Y), attenuation length (L), and steel tank reflectivity (R). Table 3 summarizes the resulting neutron efficiency (ϵ) with various combination of optical parameters. The statistical uncertainty of ϵ is computed according to binomial statistics as

$$\sigma(\epsilon) = \frac{\sqrt{(1-\epsilon)\epsilon N_{cap}}}{N_{cap}}, \quad (1)$$

in which N_{cap} is “true” n-Gd capture events in the Monte Carlo. It is $\sim 0.09\%$ for all detector conditions. In general, the agreement among the parameter space we considered is at 0.1% to 0.2% level. The largest residual systematic variation for the neutron efficiency is 0.36% between the attenuation lengths of 4.5 m and

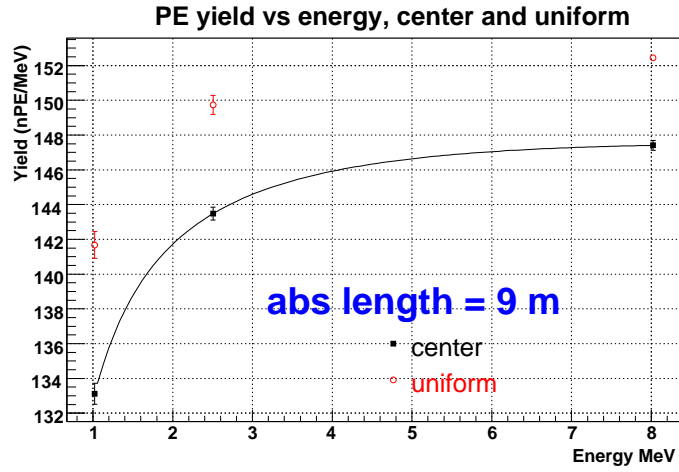


Figure 7: The PE number per MeV as a function of source energy. Black solid squares: center data; red open circles: uniform data. The black curve represents the fit of $NPE(E)$ over center data.

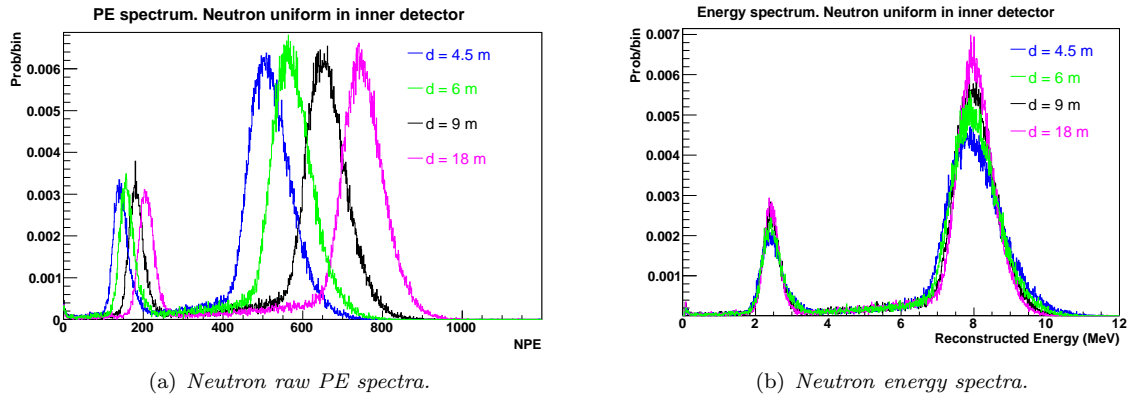


Figure 8: Neutron spectra for four different attenuation lengths (4.5, 6, 9, and 18 m): a) raw PE spectra from MC (uniform) b) reconstructed delayed energy spectra.

Y (1/MeV)	L (m)	R	Neutron Efficiency(%)
9000	9	0.8	92.76
9000	4.5	0.8	93.05
9000	6	0.8	93.03
9000	18	0.8	92.69
9000	9	0.1	92.95
9000	9	0.45	92.81
6000	9	0.8	92.87
12000	9	0.8	92.80

Table 3: Summary table of the neutron efficiency for various combination of the optical parameters using the calibration procedure described above. The “nominal” parameters are chosen as $Y = 9000/\text{MeV}$, $L=9\text{ m}$, and $R=0.8$.

18 m, as illustrated in Fig. 9 *. For a realistic variation of the attenuation, say $9 \pm 1.5\text{ m}$, the interpolated systematic variation is at the level below 0.1%.

3 Effect of various optical parameters to the positron spectrum

A typical (reconstructed) positron energy spectrum from inverse beta reaction is shown in Fig. 10. The lower edge of the spectrum is defined by two 0.511 MeV photons from e^+e^- annihilation, making ^{68}Ge an

*The cause of this effect is traced to the position dependence of the neutron yield.

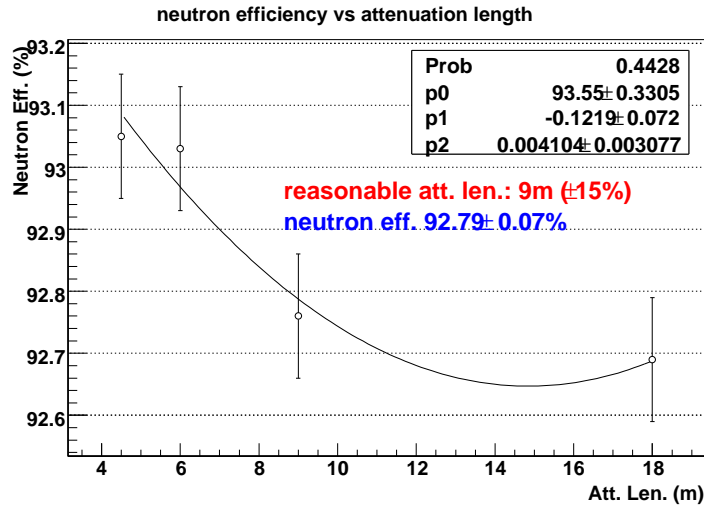


Figure 9: *The neutron efficiency for the four attenuation lengths of the liquid scintillator: 4.5, 6, 9 and 18 m. A quadratic fit is also overlaid.*

ideal source to set the energy threshold. The ^{60}Co photon energy is very close to the maximum of the spectrum, which is the natural choice for the energy scale calibrator.

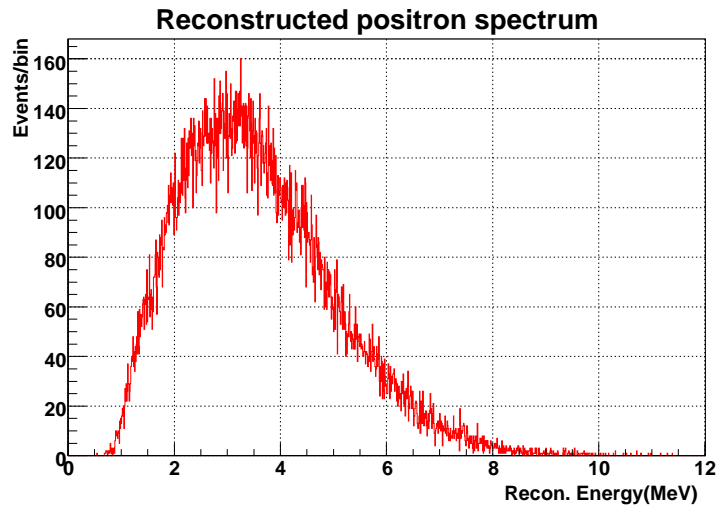


Figure 10: *A typical reconstructed positron energy spectrum.*

3.1 point-point to uniform photon yield

The measured positron spectrum is an average over the positron events uniformly distributed inside the detector. If the detector response were 100% uniform, the energy scale calibration could be trivially made by placing a ^{60}Co source at the detector center, and one could reach $< 0.1\%$ precision with 10,000 events. However, due to the position dependent response (e.g. Fig. 1), a ^{68}Ge or ^{60}Co center calibration data will need to be modified a “stretching” factor α to scale the peaks from “center” to “uniform”. This stretching factor is less an issue for the positron efficiency, but will become crucial to set the energy scale correctly to avoid fake spectrum distortion. For the neutron spectrum discussed above, the measured “uniform” n-Gd peak is used to scale the “center” calibration. Here we no longer have this self-calibrating luxury. One has to use source calibration at limited number of locations to predict the uniform response. Two simple procedures have been considered below.

In the first method, the measured yield is assumed to be an uncoupled quadratic functions of both r and z , i.e.,

$$Y(r, z) = Y_{center} + a_1 z + a_2 z^2 + b_1 r + b_2 r^2. \quad (2)$$

To demonstrate, the ^{60}Co yields at various location of along the detector “symmetry axes”, as well as the quadratic fits, are shown in Fig. 11(a). One sees that the agreements between the data and fits are good. Eqn. 2 leads to

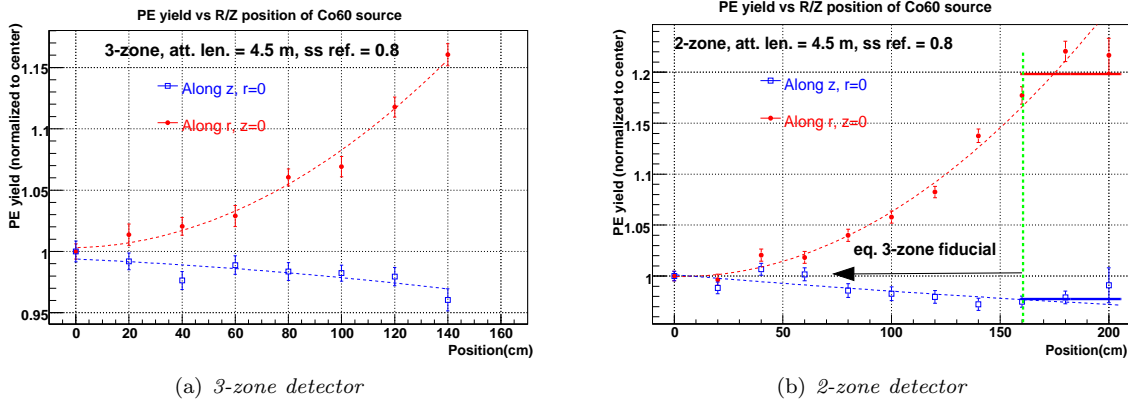


Figure 11: The ^{60}Co yield (normalized to the center yield) at various locations along r and z for a 3-zone (a) and 2-zone (b) detector. The quadratic fits are also overlaid. The scintillation yield, steel tank reflectivity, and the attenuation length in this study is taken as 9000/MeV, 0.8, and 4.5 m.

$$Y_{uniform} = Y_{center} + \frac{a_1}{2}Z + \frac{a_2}{3}Z^2 + \frac{2}{3}b_1R + \frac{b_2}{2}R^2, \quad (3)$$

in which $R = Z = 160$ cm. Therefore one can use the fits in Fig. 11(a) to calculate $Y_{uniform}$, which can then be compared with the “true” uniform yield from the simulation by putting the source uniformly throughout the target region. In Table 4, the “stretching factor” for the estimated and “true” uniform yields are listed for three different liquid scintillator attenuation lengths. One sees that the agreement is good within 1% for 12 and 18 m, and gets a little worse to 1.6% for 4.5 m.

Att. Len. (m)	3-zone		2-zone	
	$\alpha_{predicted}$	α_{true}	$\alpha_{predicted}$	α_{true}
4.5	1.088	1.071	1.088	1.058
12	1.022	1.027	1.027	1.009
18	1.015	1.021	1.037	1.016

Table 4: The predicted (based on fits in Fig. 11) and the true “stretching” factors for scintillators with different attenuation length. For comparison, the results for 2-zone and 3-zone detectors are separately listed.

A similar study can be made on a 2-zone detector. In the simulation, we made a 2-zone detector with dimensions $R=205$ cm and $Z=205$ cm (by replacing the gamma catcher with Gd-loaded liquid scintillator, and removing the inner acrylic). The ^{60}Co yield along the two axis are shown in Fig. 11(b) with quadratic fits. The detector position non-uniformity certainly increased, as compared to that of a 3-zone detector. For the positions close to the edge of the target, the ^{60}Co yield gets noisier and deviates significantly from the quadratic fit due to the “energy leakage” at the edge of the fiducial[†]. Therefore, the quadratic model in Eqn. 2 is only adopted here for vertices within the equivalent 3-zone fiducial ($r < 160$ cm and $z < 160$ cm), beyond which a flat response is taken, as indicated by the solid constant fits in Fig. 11(b). The comparison between the predicted and “true” uniform yields is summarized in the last two columns in Table 4. The predicted uniform yield is systematically 2-3% higher, mostly likely due to the fact that the yields at the detector edge away from the symmetry axes are not well-represented by our fit model. The smaller values of α_{true} (5 th column), as compared to those for a 3-zone detector (3rd column), is a pure coincidence: the (larger) position dependent yield variation happens to cancel under this specific detector model.

The method above emphasizes the yield response along the symmetry axes of the detector. Alternatively, we pursued a simpler approach to emphasize the yield response at the detector corner. We assume that the “uniform” yield can be modeled as $Y_{uniform} = (1 - a)Y_{center} + aY_{corner}$, where Y_{corner} correspond to

[†]Note, in the 2-zone case, there is no gamma catcher to alleviate the energy leakage at the edge of the fiducial.

a vertex location of $(r, z) = (140, 140)$ cm, and a is a constant between 0 and 1. We then run simulations with a source located either at the detector center or corner. By comparing these with the “uniform” yield from the simulation, a can be determined. In Table 5, the “center” and “corner” yield for detectors with various parameters have been considered, and the best value for a is 0.64 ± 0.05 with an excellent χ^2 . To view this from another perspective, let us treat $a = 0.64$ as a known “calibration” constant, and use the “center” and “corner” calibration data to predict the uniform yield. The “stretching factor” for the predicted and “true” uniform yields are listed in the last two columns of Table 4. The agreement is less than 1% for all five vastly different detectors. The study of the applicability of the same a value to other sources is underway.

detector condition	center	corner	uniform (true)	$\alpha_{predicted}$	α_{true}
att.=6 m	298.3(0.8)	311.8(1.6)	302.6(1.3)	1.050	1.046
att.=12 m	386.1(1.1)	398.6(2.7)	396.1(1.3)	1.021	1.026
ref.=0.1	180.8(0.5)	196.3(0.9)	192.0(1.0)	1.055	1.062
ref.=0.45	242.1(0.6)	258.0(1.1)	250.3(1.1)	1.042	1.034
ref.=0.8	350.0(1.0)	365.2(1.7)	360.3(1.2)	1.028	1.029

Table 5: *The simulated center, corner, and uniform yield for a ^{60}Co source with five different detector conditions. “att.” stands for liquid scintillator attenuation length, and “ref.” for the steel tank reflectivity. The change of a given detector parameter is “one-dimensional”, i.e. all other parameters were held at the nominal. The best fit of a is 0.64 ± 0.05 by combining all 5 “measurements” (see text for details). The predicted and “true” stretching factors are listed in the last two columns.*

In a real experiment, the statistical uncertainty from the source calibration will be very small. Therefore uncertainty of our knowledge of the “stretching” factor dominates the energy scale uncertainty. Based on the above two exercises, for a 3-zone detector, 1% uncertainty is achievable. For comparison, only a 2% precision is achieved for 2-zone detector using the first method. One can certainly improve the 2-zone calibration by, say, sampling more points within the fiducial. However, the increasing position non-uniformity and the energy leakage at the edge for a 2-zone detector (due to the missing gamma catcher) makes its energy scale more difficult to calibrate than that of a 3-zone detector.

3.2 Positron Efficiency

The study of positron efficiency is very similar to the study of neutron efficiency. The positron threshold is calibrated by the “center” ^{68}Ge peak location, scaled by the “stretching” factor α . The positron efficiencies thus obtained, under various sets of detector parameters, are listed in Table 6. For comparison, the efficiency values obtained using unscaled “center” ^{68}Ge peak as the lower cut are also tabulated. As one can see, using ^{68}Ge threshold, one achieves a very high positron efficiency, and the relative systematic variation among detectors (with vastly different optical parameters) is less than 0.1% level. One does not even need to scale the center calibration to the uniform to get a satisfactory relative calibration.

Y (1/MeV)	L (m)	R	e^+ Eff. (scaled Ge cut)(%)	e^+ Efficiency (unscaled Ge cut)(%)
9000	9	0.8	99.78	99.83
9000	6	0.8	99.82	99.89
9000	12	0.8	99.82	99.86
9000	9	0.1	99.80	99.89
9000	9	0.45	99.79	99.85
6000	9	0.8	99.79	99.83

Table 6: *Summary table of the positron efficiency for various combination of the optical parameters using ^{68}Ge center peak with (3rd column), and without (4th column) the stretching factor. Same as Table 3, the “nominal” parameters are chosen as $Y = 9000/\text{MeV}$, $L=9$ m, and $R=0.8$.*

3.3 Positron Spectrum Distortion

If one only wants to design the experiment to count the total number of positrons above the threshold, then the ^{68}Ge calibration from above is sufficient. On the other hand, the neutrino oscillation can also manifest as a distortion of the energy spectrum. Therefore a precise determination of the energy spectrum provides more control in the oscillation analysis. As mentioned earlier, if the energy scales of the near and far detectors have a relative difference, it can fake a spectrum distortion signal.

A ^{60}Co source at the center, scaled by the uniform/center ratio, is used to set the energy scale (2.506 MeV). This is performed on all detectors with conditions listed in Table 3. For a visual demonstration, in Fig. 12, the raw PE and the reconstructed positron energy spectra are for four representative detectors. The agreement of the energy spectra between various detectors, using such a simple calibration scheme, is quite impressive.

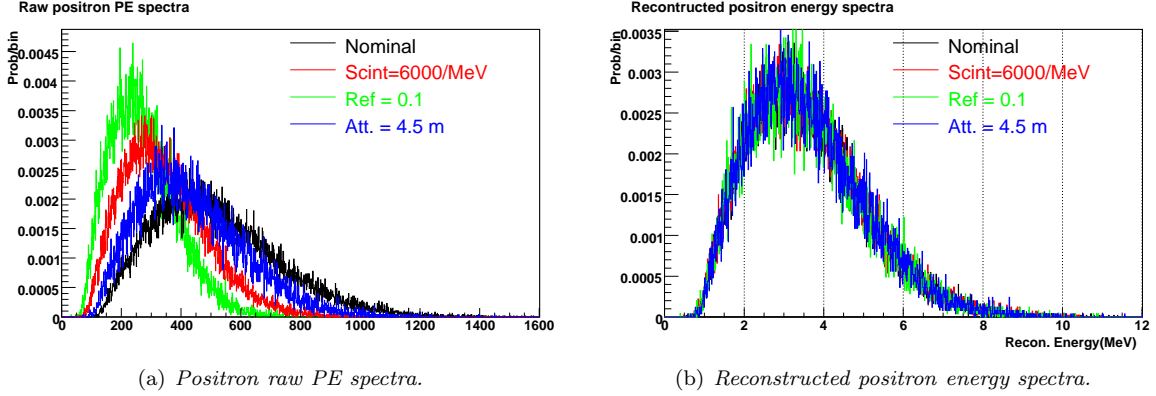


Figure 12: Positron raw PE spectra (a) and reconstructed energy spectra (b) for various detector conditions. The color code for the histograms in the figures are: [black: $Y=9000/\text{MeV}$, $L=9$ m, $R=0.8$ (nominal); red: $Y=6000/\text{MeV}$, $L=9$ m, $R=0.8$; green: $Y=9000/\text{MeV}$, $L=9$ m, $R=0.1$; and blue: $Y=9000/\text{MeV}$, $L=6$ m, $R=0.8$].

To look into the spectrum distortion, the energy spectra are rebinned into three energy bins: [1.022, 3), [3, 5), and [5, 8) MeV. The spectrum of the nominal detector is used as the reference, and the ratio of other spectrum to it are taken. The results are shown in Fig. 13. The ratios in all three energy bins for all detector conditions are consistent with zero within the statistical precision (1%-2%). Simulation with higher statistics is ongoing.

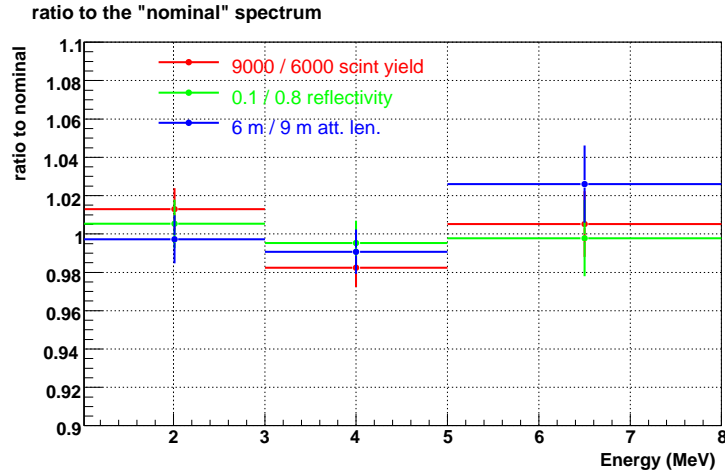


Figure 13: The ratio of the rebinned positron energy spectra of different detectors to the nominal. The color code in the figure is the same as that of Fig 10, except that there is no black (nominal) histogram in this figure.

4 Conclusion

We have made the simulation study in using the radioactive sources to calibrate a non-exhaustive list of optical parameters in the liquid scintillator. Using the calibration, a very simple vertex-independent energy spectra reconstruction scheme is considered. For both the neutron and positron energy spectra, the performance of this simple treatment is satisfactory.